




# Voltammetric determination of catechol and hydroquinone using nitrogen-doped multiwalled carbon nanotubes modified with nickel nanoparticles

Chellakannu Rajkumar<sup>1</sup> · Balamurugan Thirumalraj<sup>1,2</sup> · Shen-Ming Chen<sup>1</sup> · Pitchaimani Veerakumar<sup>3,4</sup>  · King-Chuen Lin<sup>3,4</sup>

Received: 9 April 2018 / Accepted: 23 July 2018 / Published online: 30 July 2018

© Springer-Verlag GmbH Austria, part of Springer Nature 2018

## Abstract

Nitrogen-doped multiwalled carbon nanotubes modified with nickel nanoparticles (Ni/N-MWCNT) were prepared by a thermal reduction process starting from urea and Ni(II) salt in an inert atmosphere. The nanocomposite was deposited on a screen printed electrode and characterized by X-ray diffraction, scanning and transmission electron microscopy, nitrogen adsorption, X-ray photoelectron spectroscopy, and thermogravimetric analyses. The performance of the composite was investigated by cyclic voltammetry, differential pulse voltammetry and chronoamperometry. The numerous active metal sites with fast electron transfer properties result in enhanced electrocatalytic activity towards the individual and simultaneous detection of catechol (CC) and hydroquinone (HQ), best at 0.21 V for CC and 0.11 V for HQ (vs. Ag/AgCl). For both targets the detection limit (S/N of 3) was 9 nM (CC) and 11 nM (HQ), and the Ni/N-MWCNT-electrode showed linear response from 0.1–300  $\mu\text{M}$  CC, and 0.3–300  $\mu\text{M}$  HQ. The electrode is selective over many potentially interfering ions. It was applied to the analysis of spiked water samples and gave satisfactory recoveries. It also is sensitive for CC ( $5.396 \mu\text{A} \cdot \mu\text{M}^{-1} \text{cm}^{-2}$ ) and HQ ( $5.1577 \mu\text{A} \cdot \mu\text{M}^{-1} \text{cm}^{-2}$ ), highly active, durable, acceptably repeatable and highly reproducible.

**Keywords** Nickel nanoparticles · Multiwalled carbon nanotubes · Screen printed electrode · Dihydroxybenzene isomers · Differential pulse voltammetry

## Introduction

Multiwalled carbon nanotubes (MWCNTs) have been adopted to different applications because of their cylindrical

form with  $sp^2$  carbons, composed of graphene sheets with a size of micrometer in length and nanometer in diameter [1]. Based on these characters, MWCNTs have been used for wide range applications in analytical chemistry, especially in

---

Chellakannu Rajkumar and Balamurugan Thirumalraj contributed equally to this work.

**Electronic supplementary material** The online version of this article (<https://doi.org/10.1007/s00604-018-2926-z>) contains supplementary material, which is available to authorized users.

✉ Shen-Ming Chen  
smchen78@ms15.hinet.net

Pitchaimani Veerakumar  
spveerakumar@gmail.com

King-Chuen Lin  
kclin@ntu.edu.tw

- <sup>1</sup> Department of Chemical Engineering and Biotechnology, National Taipei University of Technology, Taipei 10608, Taiwan
- <sup>2</sup> Department of Chemical Engineering, National Taiwan University of Science and Technology, Taipei 10607, Taiwan
- <sup>3</sup> Department of Chemistry, National Taiwan University, Taipei 10617, Taiwan
- <sup>4</sup> Institute of Atomic and Molecular Sciences, Academia Sinica, Taipei 10617, Taiwan

removal of environmental pollutants [2], supercapacitors [3], lithium ions batteries [4], hydrogen storage [5], and sensors [6]. However, the pristine-MWCNT structure suffers from some drawback such as limited electrocatalytic active sites and insufficient electrocatalytic behaviour during electrochemical sensing [7, 8]. Thus far, a great deal of efforts was made to tune their intrinsic properties by substituting novel heteroatoms [9, 10], which can enhance the electrocatalytic activity for generation of more active sites than the pristine-MWCNTs. To date, nitrogen-doped MWCNTs (N-MWCNTs) composites should possess high conductivity and extraordinary electrocatalytic activity. Therefore, most reports on N-MWCNTs dealt with the electrical performance of supercapacitors and electrically conductive electrodes [11]. However, to improve its electrocatalytic active sites and fast electron transfer response, incorporation of nickel or nickel oxide with N-MWCNT was verified to offer an excellent synergistic catalytic effect in electrochemical applications [12, 13]. Ni was conventionally utilized as the active electrode materials in electrochemical applications because of its outstanding catalytic ability and electrical conductivity. For instance, Ni supported MWCNT nanocomposite fabricated by one-step co-electrodeposition to detect the concentration of glucose, since it can provide a large surface area to increase the mass and electrons transfer during the reactions [14]. In particular, N-doped carbon nanotubes containing nickel nanoparticles (NiNP/NCNT) that exhibit magnetic properties favorable for product separation are desirable materials as catalysts and catalytic supports [15], and dye-sensitized solar cells [16]. In this context, the composites of Ni NPs encapsulated in N-doped carbon nanotubes (Ni/N-MWCNTs) have been used as the low-cost catalysts, which exhibit an excellent performance due to the possible geometrical, electronic, and synergistic effects in electrochemical sensing applications.

Catechol (1,2-BD; 1,2-benzenediol) and hydroquinone (HQ; 1,4-benzenediol) are two of dihydroxybenzene isomers, which are important environmental pollutants due to their high toxicity and low degradability in the ecological system [17–19]. In addition, the hydroxy aromatic compounds are found readily in the industrial effluents such as textile, paper and pulp, steel, petrochemical, petroleum refinery, rubber, dye, plastic, pharmaceutical, cosmetic, and cigarette smoke, etc. [20]. These phenolic compounds are intermediates or by-products from industry and agriculture, which are highly soluble in water; it can cause significant injury effect on the lungs, liver, kidney, DNA damage and central nervous system of living organisms [21]. Moreover, International Agency for Research on Cancer has evaluated the dihydroxybenzene isomers to be highly toxic, causing possibly carcinogenic, particularly to humans [22]. Despite their similar structures and

properties, these two dihydroxybenzene isomers have different redox properties, which usually coexist and interfere with each other during simultaneous analysis. For instance, Li and his co-workers have demonstrated a nafion-film containing cerium phosphate nanotubes-modified glassy carbon electrode (GCE) in application for the sensing of HQ, CC and resorcinol. In addition, this method was further applied to the simultaneous determination of HQ, catechol and resorcinol at 20, 134, and 572 mV vs SCE [23]. Likewise, Shen et al. have reported an electrochemical sensor based on carboxyl-functionalized carbon nanotubes in a chitosan matrix and decorated with gold nanoparticles (c-MWCNT/CTS/Au) for the simultaneous voltammetric determination of HQ and CC [23, 24]. Therefore, it is necessary to establish a fast and reliable analytical method for determination of dihydroxybenzene isomers in various matrices.

Herein, the Ni/N-MWCNT nanocomposite was prepared by thermal reduction method for simultaneous electrochemical detection of CC and HQ. We synthesized smaller sized Ni NPs embedded on the surface functionalized MWCNT. The composite material was characterized with different sophisticated analytical tools. The detection potential and peak current of CC and HQ were verified via CV and DPV. The electrochemical behavior was investigated, including CC and HQ concentration dependence, different scan rate, interference of electroactive substances and real sample analysis. Accordingly, the Ni/N-MWCNT was demonstrated to be a novel nanocomposite for electrochemical sensor for simultaneous electrochemical detection of CC and HQ with good stability, high sensitivity, and relatively wide response range.

## Experimental

### Chemicals and reagents

Nickel(II) chloride hexahydrate, ( $\text{NiCl}_2 \cdot 6\text{H}_2\text{O}$  98%), urea ( $\geq 98\%$ ), functionalized multiwalled carbon nanotubes (MWCNTs; diameter, 40–60 nm; length,  $< 2 \mu\text{m}$ ), catechol (CC,  $\geq 99\%$ ) and hydroquinone (HQ,  $\geq 99\%$ ) were bought from Tianjin Kemiou Reagent Co., Ltd. (Tianjin, China, <http://www.chemreagent.com/index.html>). Screen printed carbon electrode (SPCE) was obtained from Zensor R&D Co., LTD, Taiwan. The 0.1 M phosphate buffer (PB) solutions (pH 7) were prepared by using  $\text{Na}_2\text{HPO}_4$  (7.098 g) and  $\text{NaH}_2\text{PO}_4$  (7.8 g) in 1000 mL of water, while adjusting their pH values using 0.5 M  $\text{H}_2\text{SO}_4$  and 0.1 M NaOH solutions. All the samples were used as received without any further purification and the solutions were prepared by Milli-Q water. Detection of both HQ and CC was conducted in different water

samples which were spiked with known concentrations of HQ and CC, and then the amperometric current response was examined using standard addition method. The water samples were analyzed after filtering with filter paper (Whatman, No. 1), followed by centrifugation, and then adjusting the pH using a PB (pH 7.0).

### Preparation of Ni/N-MWCNT nanocomposite

Typically,  $\text{NiCl}_2 \cdot 6\text{H}_2\text{O}$  (2.0, 3.0, 4.0, 5.0 and 6.0 mmol) and urea (30 mmol, 1.8 g) were homogeneously dissolved in ethanol (98%) solution (100 mL) by electromagnetic stirring (800 rpm); urea was adopted as nitrogen and secondary carbon source in this fabrication of composite. Then, 500 mg of *f*-MWCNTs were mixed with the above transparent liquid under constant stirring. The mixture was dried at 80 °C until the solvent was completely evaporated. Then, the solid precursor was put into alumina boat crucible and then loaded into an electric tube furnace, which outfitted with a continuous nitrogen flow, with a temperature ramp rate of 5 °C  $\text{min}^{-1}$  until reaching the targeted temperature (800 °C), then maintained at the final temperature for 2 h. The resultant nanocomposite is denoted as Ni/N-MWCNTs. The overall preparation process and electrochemical sensing of dihydroxybenzene isomers is illustrated in Scheme 1.

### Choice of materials

Still now, different carbon nanomaterials (carbon nanotubes, carbon nanofibers, graphene, graphene oxide and carbon dots) have been utilized for electroanalytical applications owing to their high electrical conductivity and large surface area. However, they have shown insufficient active sites and result into the limited electrocatalytic active sites towards catalysis applications. Henceforth, heteroatoms (nitrogen, sulphur, phosphorus and boron) doped carbon nanomaterials have been widely used as an alternative to address those aforementioned problems. In the present work, we have synthesised N-MWCNTs and has been used for decoration of Ni on its surface. It is well-known that the transition metals, specifically Ni, Cu, Co and Fe-doped carbon materials have good catalytic activity towards various electrocatalysis/sensing applications.

However, Ni has lot of advantages over other transition metals such as high stability in neutral pH, lower capacitance current and high chemical resistance, since other transition metals (Cu and Co) are less stable in physiological pH and they most exhibited a high catalytic activity in pH over 11. Especially, Ni-doped N-MWCNTs may further increase the electrochemically active surface area (or site) of the electrocatalyst.

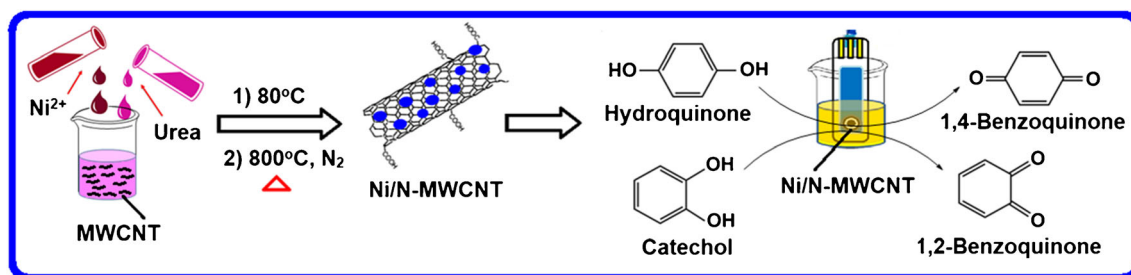
## Results and discussion

### Powder X-ray diffraction

The powder X-ray diffraction (PXRD) patterns of N-MWCNTs, and of Ni/N-MWCNT nanocomposites are shown in Fig. S1a in the Electronic Supplementary Material. The characteristic peaks at  $2\theta$  angle of  $\sim 26.2^\circ$  and  $\sim 43.1^\circ$  for *f*-MWCNT correspond to the normal structure of graphite (002) and [(100), (101)] diffraction plane (Joint Committee for Powder Diffraction Studies (JCPDS) No. 01–0646), respectively. The former peak is related to the periodicity between the graphene layers while the latter peak is in association within the graphene layer [15]. Similar findings were reported by Naeimi et al. [25]. The nickel diffraction peaks at  $2\theta = 44.6, 51.8$  and  $76.5^\circ$  can be indexed to the (111), (200) and (220) crystal planes of face-center cubic (fcc) structure of Ni, which evidenced the presence of Ni on the surface of N-MWCNTs. This suggests that the  $\text{Ni}^{2+}$  ions should be completely reduced into Ni NP during the thermal reduction and dispersed uniformly on the surface of the N-MWCNT matrix.

### $\text{N}_2$ sorption

The nitrogen ( $\text{N}_2$ ) sorption curves of the *f*-MWCNT and Ni/N-MWCNT samples are collected at 77 K (Fig. S1b). According to IUPAC classification, all samples exhibit type VI isotherm with typical small micro/macroporous nature. The sharp rise in the isotherm as the relative pressure approaches unity is due to the existence of macropores. The isotherm plots for N-MWCNT surface area were analyzed to yield ca.  $115.1 \text{ m}^2 \text{ g}^{-1}$  and pore volume  $0.0628 \text{ cm}^3 \text{ g}^{-1}$ . In



**Scheme 1** Schematic illustration of the fabrication of Ni/N-MWCNT nanocomposite and their applications

comparison, the Ni/N-MWCNT nanocomposites show slightly lower surface area ( $58.6 \text{ m}^2 \text{ g}^{-1}$ ) and pore volume ( $0.0325 \text{ cm}^3 \text{ g}^{-1}$ ), as anticipated to be caused by the immobilization of Ni NP on the surface of N-MWCNTs (Fig. S1b). The detailed textual parameter is shown in Table S1 in the Electronic Supplementary Material.

### Thermogravimetric analysis and EDX

Figure S1c in the Electronic Supplementary Material shows the thermogravimetric analysis (TGA) curves of the decomposition of N-MWCNTs and Ni/N-MWCNTs in air atmosphere. The N-MWCNT and Ni/N-MWCNT nanocomposite show a small decomposition peak at below  $200 \text{ }^\circ\text{C}$  due to the physisorbed water molecules. The N-MWCNT begins to decompose at  $\approx 520 \text{ }^\circ\text{C}$ , while the Ni/N-MWCNT nanocomposite shows two weight loss at  $205$  and  $415 \text{ }^\circ\text{C}$ , which indicate the decomposition of functional moieties in N-MWCNTs (Fig. S1c). In addition, the chemical composition of the Ni/N-MWCNT nanocomposite was verified through the measurement of energy-dispersive X-ray (EDX) analysis. Accordingly, the elements present in the Ni/N-MWCNT composite contain C (73.6%), O (20.1%), N (0.8%), and Ni (5.4%) which evidences the presence of Ni with energy bands centered at  $7.5$  and  $8.3 \text{ keV}$  (K lines) and  $0.8 \text{ keV}$  (L lines). Note that the Cu signals arise from diffuse scattering of the Cu grid support (Fig. S1d). Therefore, it is concluded that nearly all N-MWNT are decorated with NiNP [12, 26]. This fact was further supported with FE-TEM micrographs (vide-infra).

### Structural analysis

The structural changes of Ni/N-MWCNT were also investigated by scanning electron microscopy (SEM) after the thermal reduction. The SEM images of N-MWCNTs, and of the Ni/N-MWCNT nanocomposite are shown in Fig. S2, in the Electronic Supplementary Material. Based on the SEM results, the average length of N-MWCNT is  $8\text{--}15 \text{ }\mu\text{m}$  and the diameter is  $22\text{--}35 \text{ nm}$ . In addition, the transmission electron microscopy (TEM) image of N-MWCNT (Fig. S3, in the Electronic Supplementary Material) depicts bundles-like structure with smooth surface. Apparently, their sidewalls are perfectly distinguishable with diameters ranging from  $18$  to  $45 \text{ nm}$ , while the *f*-MWCNT appear highly tangled to prevent clear visualization as shown in Fig. 1c. The block spots are indicative of the formation of Ni NPs which are densely distributed on N-MWCNT surfaces with the size of NiNP approximately  $5 \pm 0.4 \text{ nm}$  (Fig. 1a,b). However, the lattice line spacing of the single Ni NP is  $0.171 \text{ nm}$  (Fig. 1c). Furthermore, the corresponding elemental mapping of C, O, N and Ni is shown in Fig. S4, in the Electronic Supplementary Material, which is also consistent with the FE-TEM observation.

### X-ray photoelectron spectroscopy

The surface properties of the Ni/N-MWCNT nanocomposite were further investigated by X-ray photoelectron spectroscopy (XPS) Fig. S5a in the Electronic Supplementary Material, which shows that the predominant species of C, O, N, and Ni elements, were visible on their surface contents. Figure S5b depicts the expanded XPS spectrum covering the C 1s spin-orbits of C-C ( $285.5 \text{ eV}$ ), C-OH ( $285.9 \text{ eV}$ ) and C=O ( $288.2 \text{ eV}$ ), respectively [26]. On the other hand, the XPS spectrum in the O 1s region gives rise to a broad single peak, comprising three deconvoluted peaks around  $534.4$ ,  $535.3$ , and  $536.3 \text{ eV}$ , which may be ascribed to the C-OH, C-O-C, and C=O functional groups, respectively (Fig. S5c). Likewise, the core level spectrum of N 1s also shows three overlapping absorption peaks at  $400.1$ ,  $401.3$ , and  $402.4 \text{ eV}$  (Fig. S5d), corresponding to the presence of pyridinic, pyrrolic, and quaternary N (or graphitic N) species. Moreover, the binding energy of the peaks at  $856.8$  and  $862.5 \text{ eV}$  corresponds to Ni  $2p_{3/2}$  and Ni  $2p_{1/2}$  spin orbitals, respectively (Fig. S5e), indicating the presence of Ni NP in the Ni/N-MWCNT nanocomposite. In contrast, the other two signals located at  $862.3 \text{ eV}$  and  $880.2 \text{ eV}$  are assigned to the satellite peaks of Ni  $2p_{3/2}$  and Ni  $2p_{1/2}$ , respectively, further revealing the presence of trace amount of Ni(II) species on the surface of Ni/N-MWCNT composite, according to previous reports [12, 15].

### Electrochemical studies

The electrocatalytic activity of Ni/N-MWCNT nanocomposite was investigated by performing cyclic voltammetry (CV) towards the simultaneous detection of CC and HQ. Figure 2a shows the CV response for bare SPCE, MWCNT, N-MWCNT and Ni/N-MWCNT or modified SPCE in  $\text{N}_2$  saturated  $0.1 \text{ M PB}$  (pH 7.0) containing  $100 \text{ }\mu\text{M}$  CC and HQ at  $50 \text{ mV s}^{-1}$  ( $-0.1$  to  $0.5 \text{ V}$  (vs. Ag/AgCl)). Notice that the MWCNTs exhibit a weak redox peak due to the limitation of both electrons transfer and mass transport. In contrast, N-MWCNT showed a well characteristic redox peak, evidencing that the doping N-atom may provide some active sites by generating a number of structure defects on the surface of the MWCNT. Further, the redox peak currents are intensively increased at modified SPCE, because of the presence of a large number of metal active sites ( $\text{Ni}^0$ ) to enhance their catalytic behaviour and conjugation of graphene  $\pi$ -system and one-pair electrons of nitrogen to improve the electron transfer process. As a result, the synergetic effects of Ni and N-MWCNT boosted the electrocatalytic activities and fast electron transfer process towards CC and HQ electrochemical reaction. In addition, the electrochemical behavior of modified SPCE was examined by CV in the absence of CC and HQ (Fig. 2b). There was no redox peak acquired in the same potential range, concluding that the planned Ni/N-MWCNT

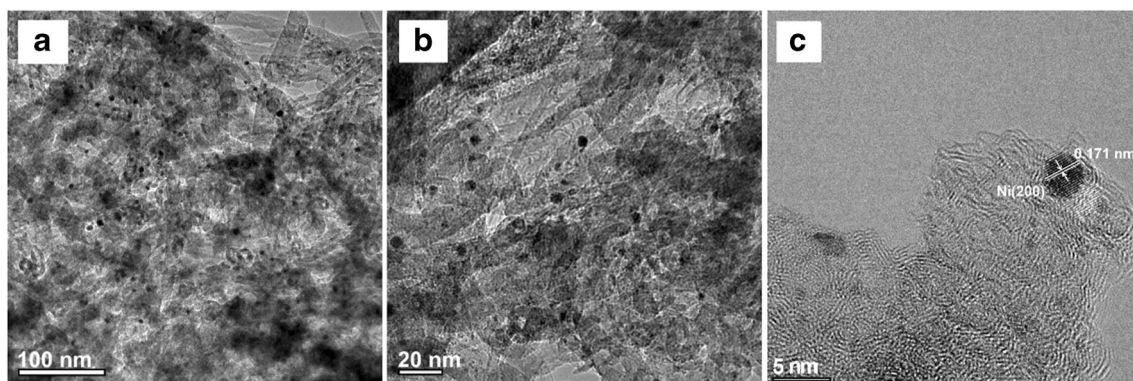


Fig. 1 TEM images of the (a-c) Ni/N-MWCNT nanocomposite with different magnification

nanocomposite offers a suitable electrode material for detection of CC and HQ. In addition, we investigated the effect of Ni loading concentration on the N-MWCNT towards CC and HQ. Thus, of Ni loading concentration (4 mM) is more efficient and effective sensing of CC and HQ under optimized conditions.

### Investigation on the electrochemical parameters

The electrochemical parameters of modified SPCE (Fig. 2c) in  $N_2$  saturated 0.1 M PB (pH 7.0) containing 100  $\mu M$  CC and

HQ were examined by CV at different scan rates (10–200  $mV s^{-1}$ ). Notice that the CC and HQ peak current were dramatically increased with increasing the scan rates from 10 to 200  $mV s^{-1}$ . The anodic peak currents ( $I_{pa}$ ) of CC and HQ offered a good linear relationship over the scan rates (Fig. 2d).

The linear regression equations were expressed as  $I_{pa} (\mu A) = 1.0538x + 17.77806$  and  $I_{pa} (\mu A) = 0.9514x + 22.006$  with a correlation coefficient  $R^2$  of 0.9964 and 0.9986 for CC and HQ, respectively. This result suggests that the electro-oxidation of CC and HQ followed surface-controlled process over the modified SPCE [27]. Furthermore, the peak potentials ( $E_{pa}$  and  $E_{pc}$ ) of CC and HQ were also shifted towards the

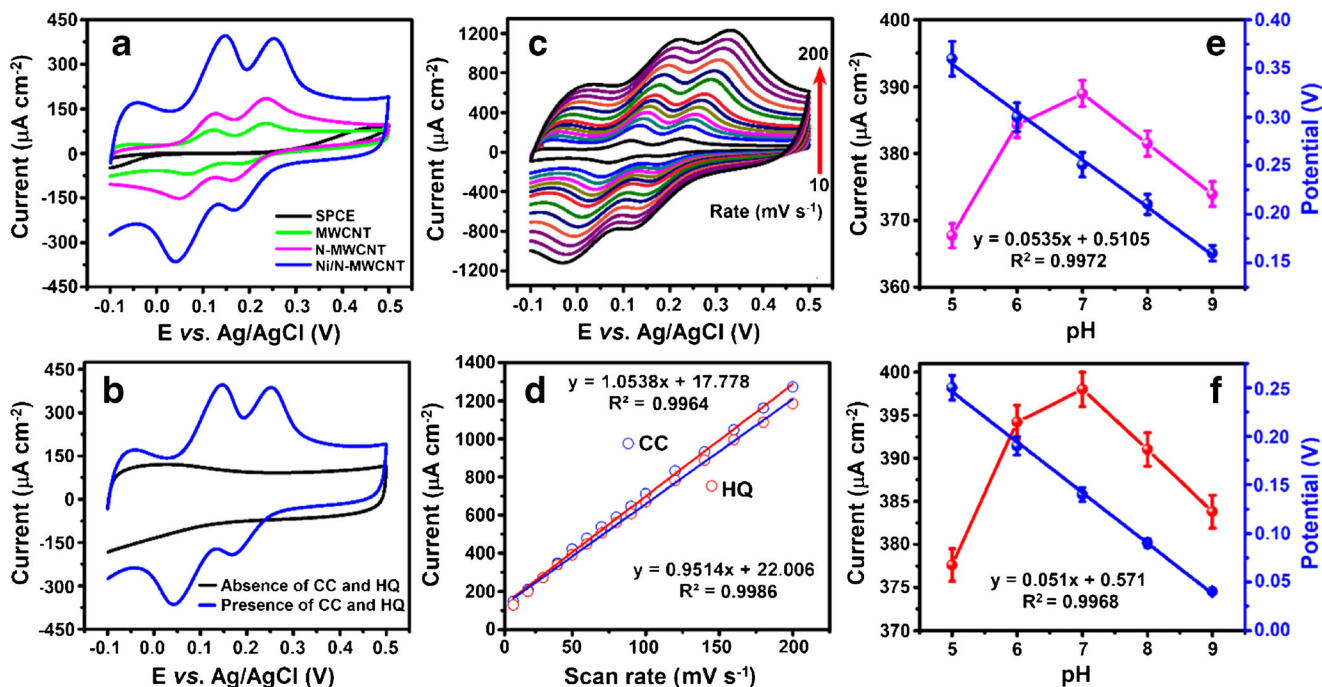


Fig. 2 a CV curves of bare SPCE, MWCNTs, N-MWCNTs, and of Ni/N-MWCNT-modified SPCE in  $N_2$  saturated 0.1 M PB (pH 7.0) containing 100  $\mu M$  CC and HQ at 50  $mV s^{-1}$  (–0.1 to 0.5 V (vs. Ag/AgCl)), b Ni/N-MWCNT-modified SPCE in the absence and presence of 100  $\mu M$  CC and HQ, at 0.21 V for CC and 0.11 V for HQ (vs. Ag/AgCl), c Ni/N-MWCNT-modified SPCE in the presence of 100  $\mu M$  CC and HQ at

different scan rates (10–200  $mV s^{-1}$ ), d plot of peak current ( $I_{pa}$ ) vs the scan rate, and (e, f) the relationship between different pH and their oxidation peak potential response of 100  $\mu M$  in CC and HQ, respectively. All measurements were conducted in  $N_2$  saturated 0.1 M PB containing 100  $\mu M$  CC and HQ at 50  $mV s^{-1}$

positive and negative directions over the pH values. Additionally, the logarithm of  $E_{pa}$  and  $E_{pc}$  presented a linearity over the pH values. Thus, the electrochemical parameters such as electron transfer co-efficient ( $k_s$ ) and charge transfer co-efficient ( $\alpha$ ) of CC and HQ may be calculated by using the following Laviron's Equation in the Electronic Supplementary Material. Accordingly,  $\alpha$  and  $k_s$  for CC and HQ are calculated to be 0.508 (CC), 0.509 (HQ) and 5.848 (CC),  $5.071 \text{ s}^{-1}$  (HQ), respectively. The obtained values of  $k_s$  and  $\alpha$  were consistent with the previous reports [28, 29].

We examine the electrocatalytic behaviour of modified SPCE in different pH range from 3 to 11. It can be seen that the achieved peak current ( $I_{pa}$ ) and peak potential ( $E_{pa}$ ) versus pH of two hydroxy benzene isomers were presented in Fig. 2e, f. When pH increased from 3 to 7, the  $I_{pa}$  of CC and HQ increased significantly to reach the maximum at pH 7. Then, a noticeable decrease in the  $I_{pa}$  of CC and HQ was found with increasing the pH values from 7 to 11. Hence, the optimal pH of this work is fixed at pH 7.

The higher concentration of hydroxyl ions at high pH might cause decrease of the adsorption capability of CC and HQ over the modified SPCE surface, resulting in the decrease in the peak current [30, 31]. Additionally, the linear plots of peak potential ( $E_{pa}$ ) of CC and HQ versus pH were expressed as  $I_{pa} (\mu\text{A}) = 0.0535 [\text{CC}] + 0.5105$  and  $I_{pa} (\mu\text{A}) = 0.051 [\text{HQ}] + 0.571$  with a correlation co-efficient  $R^2$  of 0.9972 and 0.9968 for CC and HQ, respectively. The slopes of CC and HQ are close to the theoretical prediction, according to previous report [32]. Thus, equal number of proton and electron are involved during the electrochemical reaction. Given the above results, the probable reaction mechanism of CC and HQ at modified SPCE is offered to be a two protons ( $2\text{H}^+$ ) and two electrons ( $2\text{e}^-$ ) process, as illustrated Fig. S7 in the Electronic Supplementary Material).

### Electrochemical determination of CC and HQ

To evaluate the analytical performance of the Ni/N-MWCNT nanocomposite, DPV was performed towards the individual and simultaneous detection of CC and HQ. Figure 3a displays the DPV response of CC and HQ at modified SPCE in the presence of  $0.5 \mu\text{M}$  HQ with varied concentrations of CC ranges from  $0.1$ – $142.6 \mu\text{M}$  in  $\text{N}_2$  saturated  $0.1 \text{ M}$  PB (pH 7.0) at  $50 \text{ mV s}^{-1}$ . The two significant peaks were obtained for CC and HQ, while the relative peak current ( $I_{pa}$ ) of CC was increased in linear proportion to the CC concentration (Fig. 3a<sub>1</sub>), as expressed by  $I_{pa} (\mu\text{A}) = 1.107 [\text{CC}] + 10.177$  with a correlation co-efficient ( $R^2$ ) of 0.999. The linear range of CC was estimated to be  $0.1$ – $142.6 \mu\text{M}$ . This result suggests that the modified SPCE is suitable for the simultaneous detection of CC and HQ.

Similarly, the DPV was performed with modified SPCE in the presence of  $0.5 \mu\text{M}$  CC with varied concentration of HQ

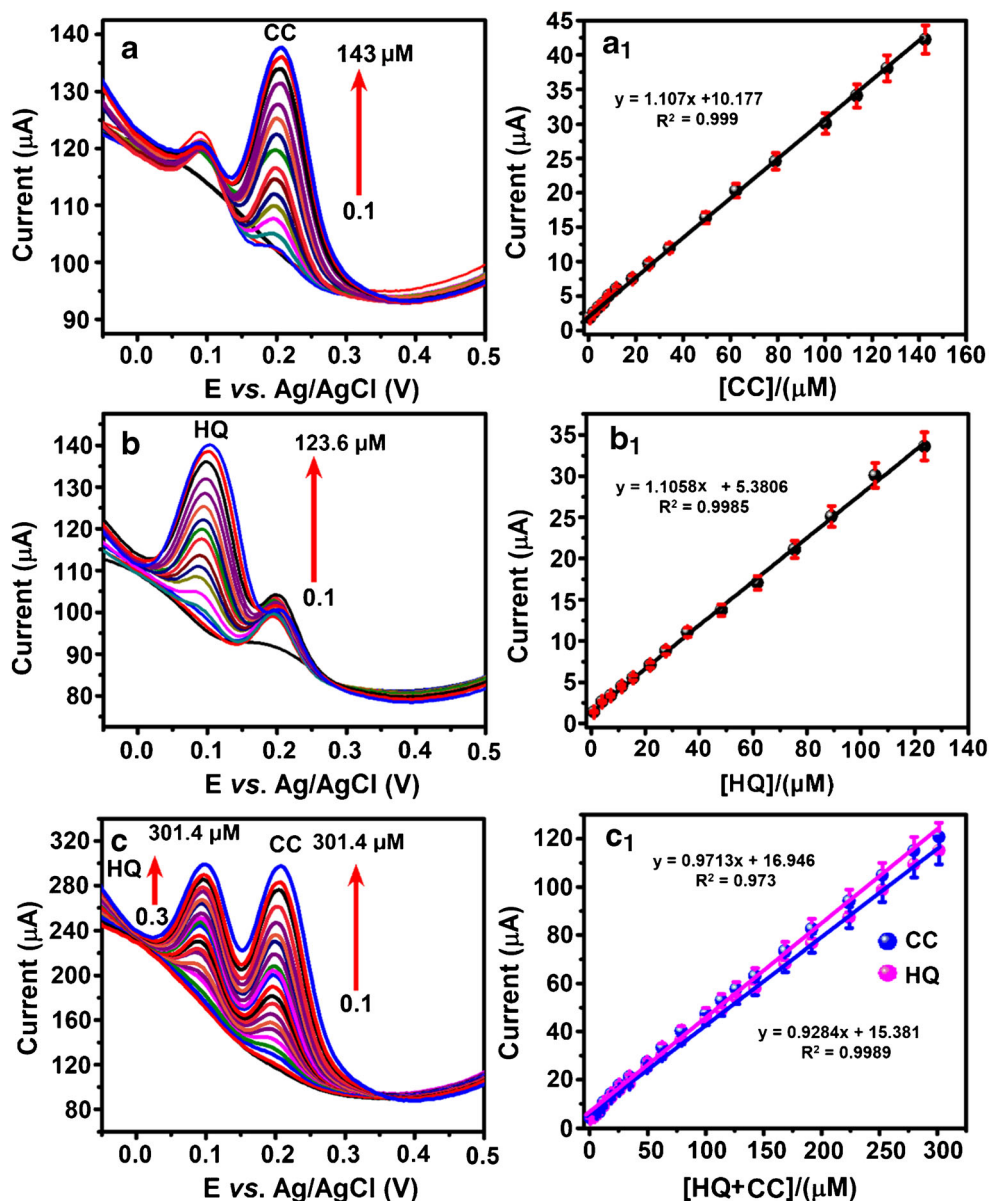
from  $0.3$ – $123.6 \mu\text{M}$  in  $\text{N}_2$  saturated  $0.1 \text{ M}$  PB (pH 7.0) at  $50 \text{ mV s}^{-1}$  is shown in Fig. 3b. The peak potential and peak current of HQ increased with increasing its concentration, independent of the interference by the fixed concentration of CC. The peak current of HQ displayed a good linear relationship over the concentration of HQ in the range of  $0.3$ – $123.6 \mu\text{M}$  with a  $R^2$  of 0.9985 (Fig. 3b<sub>1</sub>), as expressed by  $I_{pa} (\mu\text{A}) = 1.1058 [\text{HQ}] + 5.3806$ . Likewise, Fig. 3c shows the DPV response of modified SPCE in  $\text{N}_2$  saturated  $0.1 \text{ M}$  PB (pH 7.0) at  $50 \text{ mV s}^{-1}$  containing the concentrations of CC and HQ in the range of  $0.1$ – $301.4 \mu\text{M}$  and  $0.3$ – $301.4 \mu\text{M}$ , respectively. The corresponding peak currents of CC and HQ showed good linearity with the concentrations of CC and HQ (Fig. 3c<sub>1</sub>). The linear regression equations were expressed as  $I_{pa} (\mu\text{A}) = 0.9713 [\text{CC}] + 16.946$  ( $R^2 = 0.973$ ) and  $I_{pa} (\mu\text{A}) = 0.9284 [\text{HQ}] + 15.381$  ( $R^2 = 0.9989$ ) for CC and HQ, respectively. The linear range for CC and HQ was  $0.1$ – $301.4 \mu\text{M}$  and  $0.3$ – $301.4 \mu\text{M}$  with a detection limit of both  $9 \text{ nM}$  and  $11 \text{ nM}$  the electrochemical sensitivity was  $5.396 \mu\text{A } \mu\text{M}^{-1} \text{ cm}^{-2}$  and  $5.1577 \mu\text{A } \mu\text{M}^{-1} \text{ cm}^{-2}$  for HQ and CC, respectively. The results reveal that the modified electrode can be exploited for simultaneous detection of CC and HQ. Additionally, the analytical parameters such as linear range and LOD were comparable to the previously reported CC and HQ sensors is shown in Table S2 in the Electronic Supplementary Material.

### Stability, reproducibility and selectivity

The modified SPCE was examined by CV to evaluate its electrode stability, reproducibility and selectivity in detection of CC and HQ. For inspecting the storage stability, the electrode was stored in  $4 \text{ }^\circ\text{C}$  when not used. The modified SPCE was tested by CV towards the simultaneous detection of CC and HQ in  $0.1 \text{ M}$  PB every five days up to a period of 25 days as shown Fig. S8 in the Electronic Supplementary Material. The anodic peak response current, revealing a satisfactory stability for the detection of CC and HQ, indicates that our device can offers superior reproducibility as a CC and HQ sensor. The Ni/N-MWCNT-modified electrode retains 91.7% reproducibility of its initial response current of CC and HQ. Additionally, the modified SPCE achieved a relative standard deviation (RSD) of 4.3% among five independent preparation of electrodes and a RSD value of 3.8% for CC and HQ evaluated from five independent preparation of  $0.1 \text{ M}$  PB.

The selectivity of the sensor is a crucial factor for practical application. Hence, we have performed the selectivity of the sensor in the presence of some possible interfering metal ions and phenolic compounds. Figure S9 in the Electronic Supplementary Material shows the interference effect of CC and HQ in the presence of possible metal ions,  $\text{Na}^+$ ,  $\text{K}^+$ ,  $\text{Cu}^{2+}$ ,  $\text{Fe}^{3+}$ ,  $\text{Zn}^{2+}$ ,  $\text{SO}_4^{2-}$ ,  $\text{NO}_3^-$  and  $\text{Cl}^-$ ), humic acid (HA), fulvic

**Fig. 3** DPV curves for the Ni/N-MWCNT-modified SPCE in the co-presence of (a) varied [CC] in the range of 0.1–143  $\mu\text{M}$  and a fixed [HQ] of 0.1  $\mu\text{M}$ , (b) varied [HQ] in the range of 0.1–123.6  $\mu\text{M}$  and fixed [CC] of 0.5  $\mu\text{M}$ , (c) varied [CC] and [HQ] in the range of 0.1–301  $\mu\text{M}$  and 0.3–301  $\mu\text{M}$ , respectively, and their corresponding calibration plots for peak current vs. analyte concentration are depicted in  $\text{N}_2$  saturated 0.1 M PB (pH 7.0) at 0.1 to 0.5 V (vs. Ag/AgCl) (a<sub>1</sub>), (b<sub>1</sub>), and (c<sub>1</sub>), respectively



acid (FA), tannic acid (TA), and phenolic compounds such as 4-nitrophenol (4-NP) and phenol (Ph). The results show that the peak currents of CC and HQ were not interfered with by the presence of 100-fold excess addition of the given metal ions and 50-fold higher concentration of other phenolic compounds, suggesting that the good selectivity and excellent detection limit for CC and HQ in real samples.

### Water sample analysis

The dihydroxybenzene isomers easily contaminate water and affect human health and environment. Thus, we have chosen different water samples such as river water, pond water and tap water for real sample applications. The DPV was performed for the determination of CC and HQ in water samples

using a standard addition method. The obtained recovery values are shown in Table 1. The modified electrode gives acceptable recoveries, while analyzing water samples with relative standard deviations between 3.1 to 3.8% (CC) and 3.1 to 4.1% (HQ).

### Conclusion

In this work, the electrocatalytic activity of Ni/N-MWCNT nanocomposite was investigated towards the simultaneous detection of CC, and HQ by CV and DPV. On compared with other electrodes, the modified SPCE exhibited better electrocatalytic activities in the detection of CC and HQ owing to their synergistic effects of Ni and N-MWCNT. As a results, the

**Table 1** Determination of CC and HQ in different water samples using modified SPCE by DPV

Samples <sup>a</sup>	Spiked ( $\mu\text{M}$ )		Found ( $\mu\text{M}$ )		Recovery (%)		RSD <sup>b</sup> (%)	
	CC	HQ	CC	HQ	CC	HQ	CC	HQ
IWS <sub>1</sub>	50	50	49.7	49.9	99.8	99.9	3.6	3.8
IWS <sub>2</sub>	50	50	49.8	49.6	99.5	99.7	3.3	3.2
SWS <sub>1</sub>	50	50	49.4	49.7	99.2	99.4	3.2	3.4
SWS <sub>2</sub>	50	50	49.9	49.8	99.6	99.5	3.7	3.5

<sup>a</sup>IWS<sub>1</sub>: Industrial waste water sample (S<sub>1</sub>), IWS<sub>2</sub>: Industrial waste water sample (S<sub>2</sub>), SWS<sub>1</sub>: Sewage water sample (S<sub>1</sub>), SWS<sub>2</sub>: Sewage water sample (S<sub>2</sub>).

<sup>b</sup>Relative standard deviation for 3 measurements ( $n = 3$ )

detection limit (9 nM and 11 nM) linear range (0.1–301.4 and 0.3–301.4  $\mu\text{M}$ ) for CC and HQ were estimated. This electrode was also proficient to detect CC and HQ in the presence of other electroactive interfering species. Additionally, the suggested method was applied to determine CC and HQ in water samples with satisfactory results, and also this fabricated electrode showed excellent reproducibility and long-term electrode stability. These advantages made this novel electrode promising for the development of active dihydroxybenzene sensor. However, the sensor has some limitation such as selectivity in the presence of high concentration of phenolic isomers and oxygen free working environment.

**Acknowledgments** The authors are grateful for the financial support (MOST 106-2113-M-027-003-MY3 to S.M.C; MOST-102-2113-M-002-009-MY3 to KCL) from the Ministry of Science and Technology (MOST), Taiwan.

**Compliance with ethical standards** The author(s) declare that they have no competing interests.

## References

- Saeed K, Ibrahim K (2013) Carbon nanotubes—properties and applications: a review. *Carbon Lett* 14:131–144
- Ren X, Chen C, Nagatsu M, Wang X (2011) Carbon nanotubes as adsorbents in environmental pollution management: a review. *Chem Eng J* 170:395–410
- Pan H, Li J, Feng YP (2010) Carbon nanotubes for supercapacitor. *Nanoscale Res Lett* 5:654–668
- Landi BJ, Ganter MJ, Cress CD, DiLeo RA, Raffaele RP (2009) Carbon nanotubes for lithium ion batteries. *Energy Environ Sci* 2: 638–654
- Wang Y, Li A, Wang K, Guan C, Deng W, Lia C, Wang X (2010) Reversible hydrogen storage of multi-wall carbon nanotubes doped with atomically dispersed lithium. *J Mater Chem* 20:6490–6494
- Agui L, Yáñez-Sedeno P, Pingarron JM (2008) Role of carbon nanotubes in electroanalytical chemistry: a review. *Anal Chim Acta* 622:11–47
- Lin JY, Lien CH, Chou SW (2012) Multi-wall carbon nanotube counter electrodes for dye-sensitized solar cells prepared by electrophoretic deposition. *J Solid State Electrochem* 16:1415–1421
- Lee WJ, Ramasamy E, Lee DY, Song JS (2009) Efficient dye-sensitized solar cells with catalytic multiwall carbon nanotube counter electrodes. *ACS Appl Mater Interfaces* 1:1145–1149
- Shrestha A, Batmunkh M, Shearer CJ, Yin Y, Andersson GG, Shapter JG, Qiao S, Dai S (2017) Nitrogen-doped CNx/CNTs heteroelectrocatalysts for highly efficient dye-sensitized solar cells. *Adv Energy Mater* 7:1602276–1602284
- Lee JM, Lim J, Lee N, Park HI, Lee KE, Jeon T, Nam SA, Kim J, Shin J, Kim SO (2015) Synergistic concurrent enhancement of charge generation, dissociation, and transport in organic solar cells with plasmonic metal-carbon nanotube hybrids. *Adv Mater* 27: 1519–1525
- Ramesh S, Sivasamy A, Kim HS, Kim JH (2017) High-performance N-doped MWCNT/GO/cellulose hybrid composites for supercapacitor electrodes. *RSC Adv* 7:49799–49809
- Gund GS, Dubal DP, Shinde SS, Lokhande CD (2014) Architected morphologies of chemically prepared NiO/MWCNTs nanohybrid thin films for high performance supercapacitors. *ACS Appl Mater Interfaces* 6:3176–3188
- Dhvale VM, Gaikwad SS, George L, Devi RN, Kurungot S (2014) Nitrogen-doped graphene interpenetrated 3D Ni nanocages: efficient and stable water-to dioxigen electrocatalysts. *Nanoscale* 6: 13179–13187
- Sun A, Zheng J, Sheng Q (2012) A highly sensitive non-enzymatic glucose sensor based on nickel and multi-walled carbon nanotubes nanohybrid films fabricated by one-step co-electrodeposition in ionic liquids. *Electrochim Acta* 65:64–69
- Yao Y, Zhang J, Chen H, Yu M, Gao M, Hu Y, Wang S (2018) Ni<sup>0</sup> encapsulated in N-doped carbon nanotubes for catalytic reduction of highly toxic hexavalent chromium. *Appl Surf Sci* 440:421–431
- Chen M, Zhao G, Shao LL, Yuan ZY, Jing QS, Huang KJ, Huang ZY, Zhao XH, Zou GD (2017) Controlled synthesis of nickel encapsulated into nitrogen-doped c nanotubes with covalent bonded interfaces: the structural and electronic modulation strategy for an efficient electrocatalyst in dye-sensitized solar cells. *Chem Mater* 29:9680–9694
- Hirakawa K, Oikawa S, Hiraku Y, Hirokawa I, Kawanishi S (2002) Catechol and hydroquinone have different redox properties responsible for their differential DNA-damaging ability. *Chem Res Toxicol* 15:76–82
- Guo Q, Huang J, Chen P, Liu Y, Hou H, You T (2012) Simultaneous determination of catechol and hydroquinone using electrospun carbon nanofibers modified electrode. *Sensors Actuators B Chem* 163: 179–185
- Velmurugan M, Karikalan N, Chen SM, Cheng YH, Karupiah C (2017) Electrochemical preparation of activated graphene oxide for the simultaneous determination of hydroquinone and catechol. *J Colloid Interface Sci* 500:54–62
- Wei C, Huang Q, Hu S, Zhang H, Zhang W, Wang Z, Zhu M, Dai P, Huang L (2014) Simultaneous electrochemical determination of hydroquinone, catechol and resorcinol at nafion/multi-walled carbon nanotubes/carbon dots/multi-walled carbon nanotubes modified glassy carbon electrode. *Electrochim Acta* 149:237–244
- Joseph P, Klein-Szanto AJP, Jaiswal AK (1998) Hydroquinones cause specific mutations and lead to cellular transformation and in vivo tumorigenesis. *Br J Cancer* 78:312–320
- IARC Working Group IARC Monographs (1999) on the evaluation of carcinogenic risks to humans. IARC, Lyon, France. 71 Part 2: 433–451
- Shen Y, Rao D, Sheng Q, Zheng J (2017) Simultaneous voltammetric determination of hydroquinone and catechol by using a glassy carbon electrode modified with carboxy-functionalized carbon nanotubes in a chitosan matrix and decorated with gold nanoparticles. *Microchim Acta* 184:3591–3601
- Li Z, Yue Y, Hao Y, Feng S, Zhou X (2018) A glassy carbon electrode modified with cerium phosphate nanotubes for the



- simultaneous determination of hydroquinone, catechol and resorcinol. *Microchim Acta* 185:215
25. Naeimi H, Dadaei M (2015) Functionalized multi-walled carbon nanotubes as an efficient reusable heterogeneous catalyst for green synthesis of N-substituted pyrroles in water. *RSC Adv* 5:76221–76228
  26. Veerakumar P, Chen SM, Madhu R, Veeramani V, Hung CT, Liu SB (2015) Nickel nanoparticle-decorated porous carbons for highly active catalytic reduction of organic dyes and sensitive detection of hg(II) ions. *ACS Appl Mater Interfaces* 7: 24810–24821
  27. Nasr A, Cañizares P, Sáez C, Lobato J, Rodrigo MA (2005) Electrochemical oxidation of hydroquinone, resorcinol, and catechol on boron-doped diamond anodes. *Environ Sci Technol* 39: 234–7239
  28. Zhang W, Zheng J, Lin Z, Zhong L, Shi J, Wei C, Zhang H, Hao A, Hu S (2015) Voltammetric determination of catechol and hydroquinone at poly (niacinamide) modified glassy carbon electrode. *Anal Methods* 7:6089–6094
  29. Chen D, Zhou H, Li H, Chen J, Li S, Zheng F (2017) Self-template synthesis of biomass-derived 3D hierarchical N-doped porous carbon for simultaneous determination of dihydroxybenzene isomers. *Sci Rep* 7:14985
  30. Cui S, Li L, Ding Y, Zhang J (2016) Mesoporous cobalto-cobaltic oxide modified glassy carbon electrode for simultaneous detection of hydroquinone and catechol. *J Electroanal Chem* 782:225–232
  31. Yin H, Zhang Q, Zhou Y, Ma Q, Liu T, Zhu L, Ai S (2011) Electrochemical behavior of catechol, resorcinol and hydroquinone at graphene–chitosan composite film modified glassy carbon electrode and their simultaneous determination in water samples. *Electrochim Acta* 56:2748–2753
  32. Silva ARL, Santos AJ, Martínez-Huitle CA (2018) Electrochemical measurements and theoretical studies for understanding the behavior of catechol, resorcinol and hydroquinone on the boron doped diamond surface. *RSC Adv* 8:3483–3492